an Agilent G1607A CE–electrospray ionization (ESI)–MS sprayer kit (Agilent Technologies). For system control and data acquisition, we used Agilent G2201AA ChemStation software for CE and Analyst QS for TOFMS.

For measuring nucleotide derivatives, we used a CE-ESI-quadrupole MS system composed of an Agilent 1100 series MSD mass spectrometer equipped with the aforementioned other instruments. For the control and data acquisition in this system, we used Agilent 3D CE-MSD ChemStation software.

CE-TOFMS Conditions for Cationic Metabolite Analysis

Cationic metabolites were separated in a fused-silica capillary (50 μm i.d. × 100 cm total length) filled with 1 mol/L formic acid as the reference electrolyte (16). Sample solution was injected at 50 mbar for 3 s (~3 nL), and positive voltage of 30 kV was applied. The capillary and sample trays were maintained at 20°C and below 5°C, respectively. Sheath liquid that comprised methanol/water (50% v/v) that contained 0.5 μmol/L reserpine was delivered at 10 μL/min. ESI-TOFMS was operated in the positive ion mode. The capillary voltage was set at 4 kV and a flow rate of nitrogen gas (heater temperature 300°C) was set at 10 psig. In TOFMS, the fragmenter voltage, skimmer voltage, and octapole radio frequency voltage (Oct RFV) were set at 75, 50, and 125 V, respectively. An automatic recalibration function was performed by using two reference masses of reference standards; protonated methanol dimer ($[2\text{ methanol}+H]^+$, *m/z* 65.059706) and protonated reserpine ($[M+H]^+$, *m/z* 607.280659), which provided the lock mass for exact mass measurements. Exact mass data were acquired at the rate of 1.5 cycles/s over a 50 to 1,000 *m/z* range.

CE-TOFMS Conditions for Anionic Metabolite Analysis

Anionic metabolites were separated in a cationic-polymer–coated SMILE(+) capillary (Nacalai Tesque) filled with 50 mmol/L ammonium acetate solution (pH 8.5) as the reference electrolyte (13). Sample solution was injected at 50 mbar for 30 s (~30 nL) and a negative voltage of −30 kV was applied. Ammonium acetate (5 mmol/L) in 50% methanol/water (50% v/v) that contained 1 μmol/L reserpine was delivered as sheath liquid at 10 μL/min. ESI-TOFMS was operated in the negative ion mode. The capillary voltage was set at 3.5 kV. In TOFMS, the fragmenter voltage, skimmer voltage, and Oct RFV were set at 100, 50, and 200 V, respectively. An automatic recalibration function was performed by using two reference masses of reference standards: deprotonated acetate dimer ($[2M-H]^-$, *m/z* 119.034984) and deprotonated reserpine ($[M-H]^-$, *m/z* 607.266107). Other conditions were identical to those used in cationic metabolome analysis.

CE-MS Conditions for Nucleotide-Related Metabolite Analysis

Separations were carried out in a fused-silica capillary (50 μm i.d. × 100 cm total length) filled with 50 mmol/L ammonium acetate solution (pH 7.5) as electrolyte (17). Before the first use, a new capillary was pretreated with preconditioning buffer, 25 mmol/L ammonium acetate/75 mmol/L sodium phosphate solution (pH 7.5), for 20 min. Before each injection, the capillary was equilibrated by flushing with the preconditioning buffer for 10 min and subsequently with the running buffer for 6 min, which was replenished every run using a buffer replenishment system equipped with the Agilent CE. Sample solution was injected at 50 mbar for 30 s (~30 nL). A voltage of +30 kV was applied and a pressure of 50 mbar was applied to the inlet capillary during the run (17). The capillary temperature was maintained at 20°C, and the sample tray was cooled to below 5°C. Ammonium acetate (5 mmol/L) in 50% methanol/water (v/v) was delivered as the sheath liquid at 10 μL/min. ESI-quadrupole MS was operated in the negative ion mode, and the capillary voltage was set at 3.5 kV. A flow of heated dry nitrogen gas (heater temperature 300°C) was switched off during the preconditioning step, and a pressure of 10 psig was applied 0.1 min after sample injection. Compounds were monitored using selective ion monitoring mode.

Liquid Chromatography Tandem Mass Spectrometry Conditions for Glucose Quantification

Liquid chromatography tandem mass spectrometry experiments were performed using an Agilent 1100 series HPLC system and an API3000 triple-quadrupole tandem mass spectrometer (Applied Biosystems), with the Applied Biosystems Analyst software for data acquisition. The separation was carried out on a TSKgel Amide-80 column (2.1 mm i.d. × 25 cm; Tosoh) and the mobile phase consisted of 75% acetonitrile and 25% Milli-Q water at a flow-rate of 0.2 mL/min. The temperature of the column oven was set at 80°C and 1-μL aliquots of the sample solution were injected into the column. Turbo spray mode was selected in the negative ion mode. Nebulizer gas pressure, air curtain gas pressure, nitrogen turbo gas temperature, and ion spray voltage were set at 12 psig, 6 psig, 500°C, and −4.5 kV, respectively. Multiple reaction monitoring detection was performed in MS/MS analysis to obtain sufficient selectivity and sensitivity.

CE-TOFMS Data Processing

Raw data were processed using in house software for the quantitation of metabolites. The overall data processing flow consists of the following steps; noise-filtering, baseline-correction, migration time alignment, peak detection, and integration of peak area from a 0.02 *m/z*-wide slice of the electropherograms, which resemble the strategies used in widely used data processing software for LC-MS and GC-MS data analysis such as MassHunter (Agilent Technologies) and XCMS (18). Subsequently, the accurate *m/z* of each peak was calculated by Gaussian curve fitting in the *m/z* domain, and migration times were normalized using alignment algorithms based on dynamic programming (15, 19). All target metabolites were identified by matching their *m/z* values and migration times with those of the standard compounds. Processed peak lists were exported for further statistical analysis.

Statistical Analysis

For each sample, the measured metabolite concentrations were normalized using tissue weight to obtain the amount of metabolite contained per gram of each sample. The Wilcoxon matched pairs test was used to compare metabolite levels in tumor and nontumor groups, to determine statistical significance. Z-score normalization was performed and heat maps of metabolite levels were generated using hierarchical clustering based on Pearson correlation coefficients using the MultiExperiment Viewer (MeV) software (Institute for Genomic Research; ref. 20).

Results and Discussion

Metabolome analyses of colon and stomach cancer tissues. We obtained pairs of surgically resected tumor and surrounding normal tissue samples from 16 colon and 12 stomach cancer patients and extracted metabolites for metabolome analysis. Surgically excised tissue samples were immediately frozen in liquid nitrogen, quickly weighed and immersed in methanol with internal standards, and completely homogenized at 2°C, which thus minimized sample degradation and halted potential enzymatic reactions during metabolite extraction process.

The CE-TOFMS systems in three different modes for cation, anion, and nucleotide analyses detected 738 (normal) and 877 (tumor) peaks in colon and 1007 (normal) and 1142 (tumor) peaks in stomach tissues on average, after eliminating redundant peaks, such as spike noises, fragments, and adduct ions. Among these, 94 peaks in colon and 95 peaks in stomach were identified and quantified with metabolite standards by matching the closest *m/z* values and normalized migration times for further statistical comparisons and interpretations. The identified metabolites and their quantities are listed in Supplementary Table S1 and graphically represented on a large-scale metabolome map (Supplementary Fig. S1).

The relative levels of metabolites in normal and tumor tissues obtained from colon and stomach cancer patients were visualized by using a hierarchical clustering algorithm (Supplementary Fig. S2). The normalized metabolome data were clustered according to metabolites vertically and samples horizontally. Two distinct metabolite clusters were observed in colon tissues: Most

metabolite levels including glycolytic intermediates, amino acids, some TCA and urea cycle intermediates, and nucleosides were higher in tumor tissues compared with their normal counterparts; however, these clusters were less distinguishable in stomach tissues. This trend was also present in the sample clusters: Colon samples were clearly separated into tumor and normal groups except for one normal sample clustered within the tumor group, whereas stomach samples were not well-separated. This indicates that tumor and normal stomach tissues were less distinguishable compared with colon tissues, according to the metabolome data obtained in this study. However, several key metabolites in energy metabolism, such as glucose and nucleoside triphosphates, were lower in both colon and stomach tumor tissues. No significant correlation was found between metabolite levels and the cancer stages of patients in both tissue types (data not shown).

Glycolysis and TCA cycle. As expected from the notion that cancer cells can deplete glucose in the hypovascular microenvironment caused by the hyperactivity of glycolysis, glucose concentrations were much lower in tumor than normal tissues in both types of cancers (Fig. 2). Mean glucose concentration of normal and tumor tissues was 1,220 ± 150 (mean ± SE) and 123 ± 43 nmol/g, respectively, in colon (P = 0.0005) and 1,290 ± 168 and 424 ± 131 nmol/g, respectively, in stomach (P = 0.0068) tissues. Concentrations of metabolites that are involved in glycolysis, pentose phosphate pathway, and TCA cycle are illustrated on a metabolic pathway map in Fig. 3. In colon and stomach cancer, tumor tissues contained nearly equal or higher amounts of glycolytic intermediates than their corresponding normal counterparts, and this trend was clearer in colon tissues. Scarce glucose and modest glucose 6-phosphate concentrations might result from the overexpression of glucose transporters (21) and particularly type II hexokinase expression (22), which are frequently observed in colon and stomach cancer. The accumulation of glucose 1-phosphate in colon cancer is also intriguing in that glycogen synthase kinase 3β expression is reportedly higher in colon cancer cell lines and colorectal cancer patients compared with their respective normal counterparts (23), which may result in the enhancement of glycogenolysis and a continuous supply of glucose 6-phosphate.

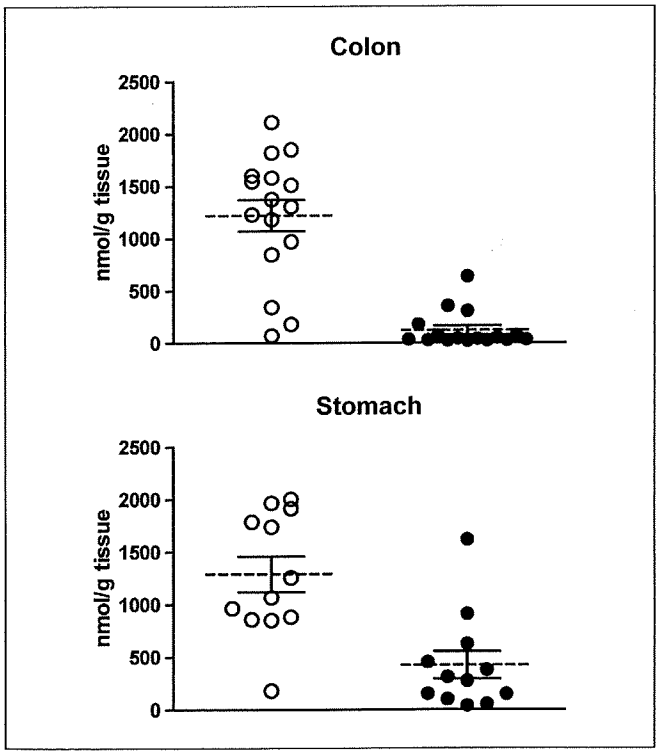

Figure 2. Quantified glucose concentrations of colon and stomach tissue samples. These data are individual glucose concentrations of normal and tumor samples each of colon and stomach subjects, with the mean concentrations (*dotted line*) ± SE.

In addition, pyruvate concentration is significantly lower in colon tumor and slightly lower in stomach tumor tissues, whereas lactate concentration in tumor tissues is higher in both tumor types than in their corresponding normal counterparts. This clearly indicates a high dependence of cancer cells on anaerobic breakdown of pyruvate. In particular, high lactate dehydrogenase 5 activity and resulting effective conversion of pyruvate to lactate have been identified in colon cancer (24, 25). Active glycolysis also increases the cytosolic NADH/NAD^+ ratio and thereby accelerates the activity of lactate dehydrogenase (26). Enhanced pyruvate-to-lactate conversion may also be due to the activation of pyruvate dehydrogenase kinase, isozyme 1 (PDK1) in cancer cells, which inactivates pyruvate dehydrogenase and leads to inactivation of the TCA cycle in cancer cells (27). Moreover, lactate accumulation creates a potentially favorable microenvironment for cancer cells to proliferate, as it causes local acidosis and potentially modulates the activity of proteases that decompose extracellular matrix, thereby liberating peptides and amino acids that are consumable for energy generation (28). Therefore, it is likely that cancer cells preferentially use glucose because of their intrinsic metabolic characteristics and microenvironmental aspects such as hypoxia. Moreover, extremely low glucose content in tumor tissues might result from poor blood supply and high glucose consumption by cancer cells.

If the density of soft tissues is assumed as 1 g/mL, our data indicate that the glucose concentration in tumor tissues is only ~1 of 45 (colon) or 1 of 13 (stomach) of the typical blood glucose concentration (1 mg/mL or 5.6 mmol/L). When cultured cancer cells are deprived of glucose, most conventional cytotoxic anticancer agents significantly lose their effectiveness (29). This is important when the pharmacologic effects of anticancer agents in the actual tumor microenvironment are considered since it was found to be significantly different from the typical glucose-rich medium that is commonly used for *in vitro* experiments. Accordingly, the present data imply that responses of most colon and stomach cancer cells against conventional anticancer drugs under the actual nutritionally poor *in vivo* environment could be considerably different from that which we expect from the data obtained under typical culture conditions.

Unexpectedly, significant organ-specific differences were also observed in the metabolite levels of the initial part of the TCA cycle, including acetyl CoA, citrate, *cis*-aconitate, iso-citrate, and 2-oxoglutarate, which were markedly lower in colon tissues. Interestingly, however, levels of the three TCA metabolites succinate, fumarate, and malate were comparable in colon and stomach tissues, whereas they were significantly higher in tumor samples in both cancers (Fig. 3). Wiesner and colleagues (30) have shown a decrease of citrate and 2-oxoglutarate and an increase of malate and succinate in anoxic rat heart myocytes. The trend of these TCA intermediate levels is consistent with our data obtained from colon tissues, presumably representing a typical metabolic fingerprint of hypoxic cells. In contrast, abundant TCA

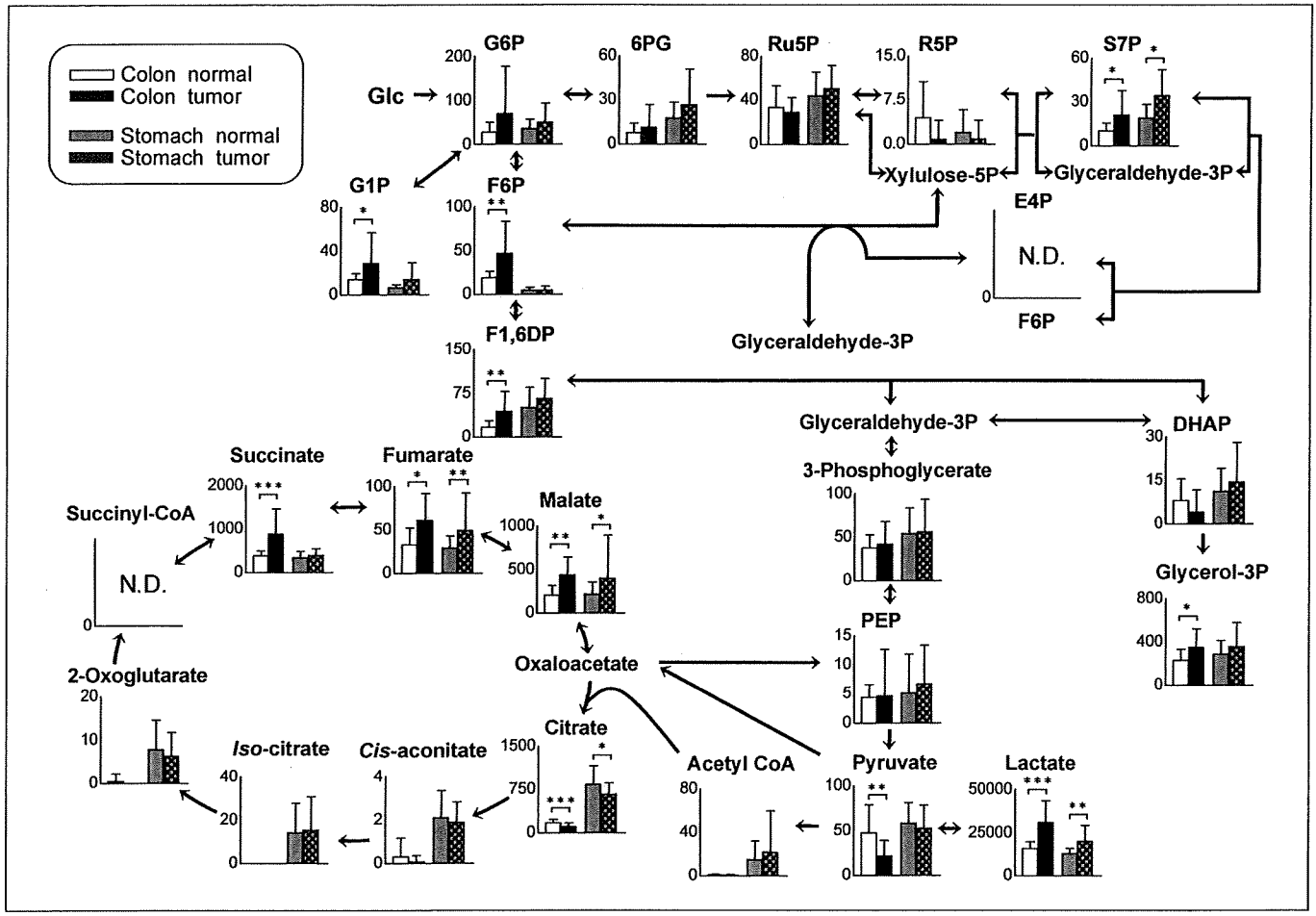

Figure 3. Quantified levels of metabolites involved in central carbon metabolism. Metabolite concentrations of colon and stomach tissues superimposed on a metabolic pathway map that included glycolysis, and the pentose phosphate and TCA pathways. *Columns,* average concentration (nmol/g tissue); *bars,* SD. *N.D.,* the metabolite concentration was below the detection limit of the analysis. All the *P* values were evaluated by the Wilcoxon matched pair test. *, $P < 0.05$; **, $P < 0.01$; ***, $P < 0.001$.

intermediates in stomach tissues, regardless of whether from tumor or normal tissues, imply active aerobic respiration via oxidative phosphorylation. It is uncertain, however, what causes the accumulation of fumarate and succinate in colon cancer tissues, despite extremely low concentrations of other TCA intermediates such as citrate and 2-oxoglutarate. In fact, it is known that some parasites and bacteria synthesize ATP without oxygen by using a reverse reaction of succinate dehydrogenase and produce succinate as a byproduct, which is so-called fumarate respiration, in which fumarate rather than molecular oxygen is used as electron acceptor (31, 32). Although the capability of mammalian cells to use fumarate respiration as an ATP generator has not been confirmed yet, we obtained strong evidence that the energy generation of cancer cells greatly depends on fumarate respiration under conditions of glucose deprivation and severe hypoxia.[3] Our data uncovered the metabolically unfavorable microenvironment of tumor tissues characterized by extremely low glucose availability under relatively hypoxic conditions in which the cells apparently rely on minimal aerobic respiration via the TCA cycle. Hence, the active use of fumarate respiration by cancer cells provides a likely and intriguing explanation for the accumulation of fumarate and succinate observed in colon tumor tissues.

Amino acids and nucleotides. Availability of amino acids is pivotal for cell proliferation because cancer cells are known to use some amino acids as energy sources (26). Free amino acids are mostly supplied to tissues via the bloodstream; thus, if blood supply to cancer tissues is considerably limited, amino acid content in tumor tissues may be lower compared with that in their normal counterparts. However, contrary to our expectations, levels of most amino acids and their primary derivatives were significantly higher in tumors than in normal colon and stomach tissues (Fig. 4). Among all the amino acids, however, an exception was glutamine; the colon and stomach tumor content of which was nearly equal to that in normal tissues. It has been pointed out that glutamine is a preferred amino acid for energy generation by cancer cells (33). High glutaminase activity and low glutamine synthase activity have been observed in several types of cancer cells (34). Because glutamate is the most abundant amino acid in tumor tissues, the conversion of glutamine to glutamate might be enhanced in tumor tissues.

One obvious question raised is the origin of these amino acids. Under limited blood supply, two main sources of amino acids can

[3] K. Kami et al. submitted for publication.

be conceived: one is the degradation of extracellular matrix particularly by matrix metalloproteinases and the other is the autophagic degradation of preexisting intracellular proteins. In this perspective, it is notable that hydroxyproline concentration was significantly higher in tumor tissues than in their normal counterparts (P = 0.0005 in colon and P = 0.0025 in stomach tissues). Hydroxyproline is abundant in collagen and is posttranslationally produced from proline, which suggests that the higher concentration of hydroxyproline in tumor tissues is indicative of excess degradation of collagen (35). Autophagy is another possible source of amino acids, as it is well-documented that autophagy liberates and thereby increases the free amino acid pools (36, 37). We also have found recently that autophagy seems essential for colon cancer cell survival (38) and is highly active in colon and pancreatic cancers (38, 39). Up-regulation of amino acid biosynthesis per se does not explain the accumulation of all the essential amino acids observed in tumor tissues. One might argue that all the amino acid levels seem to be higher in tumors because the number of cells contained in tumor tissues might have been greater than that in normal tissues, as cancer cells may have been highly aggregated. To rule out this possibility, we extracted DNA simultaneously with metabolites from each tissue and normalized our metabolome data with respect to the DNA content of each sample, and confirmed that the trend in amino acid levels did not change (data not shown).

The levels of most nucleotides such as ATP, ADP, GTP, and GDP in tumor and normal colon tissues were significantly lower than those in stomach tissues (Fig. 4). Nevertheless, no significant difference between colon and stomach tissues was observed with regard to the average adenylate energy charge (40), which is evaluated by the equation, [(ATP)+1/2(ADP)]/[(ATP)+(ADP)+(AMP)]. The low levels of most purine and pyrimidine compounds in colon tissues may indicate a relatively slower colon cell growth compared with stomach cells, as a recent study has shown that the nucleotide pools continuously decrease as the growth stage moves from the exponential to stationary phase in *Escherichia coli* (41). A challenging but intriguing alternative is that the levels of nucleotide pools may reflect the oxygen availability and its dependency in each tissue because hypoxic stress has been found to reduce purine and pyrimidine pools (42). The high-energy charge in colon tissues, despite the low total adenylate level, might be maintained by AMP deaminase reaction, which is known to stabilize the energy charge by decomposing adenylate (43). It is, however, remarkable that no significant difference between tumor and normal tissues was found for most nucleotide phosphates, total adenylate, and energy charge in either colon or stomach tissues. This implies that cancer cells have a growth advantage over their normal counterparts, not by securing more ATP and other building blocks for DNA synthesis, but rather by efficiently exploiting some strategic energy

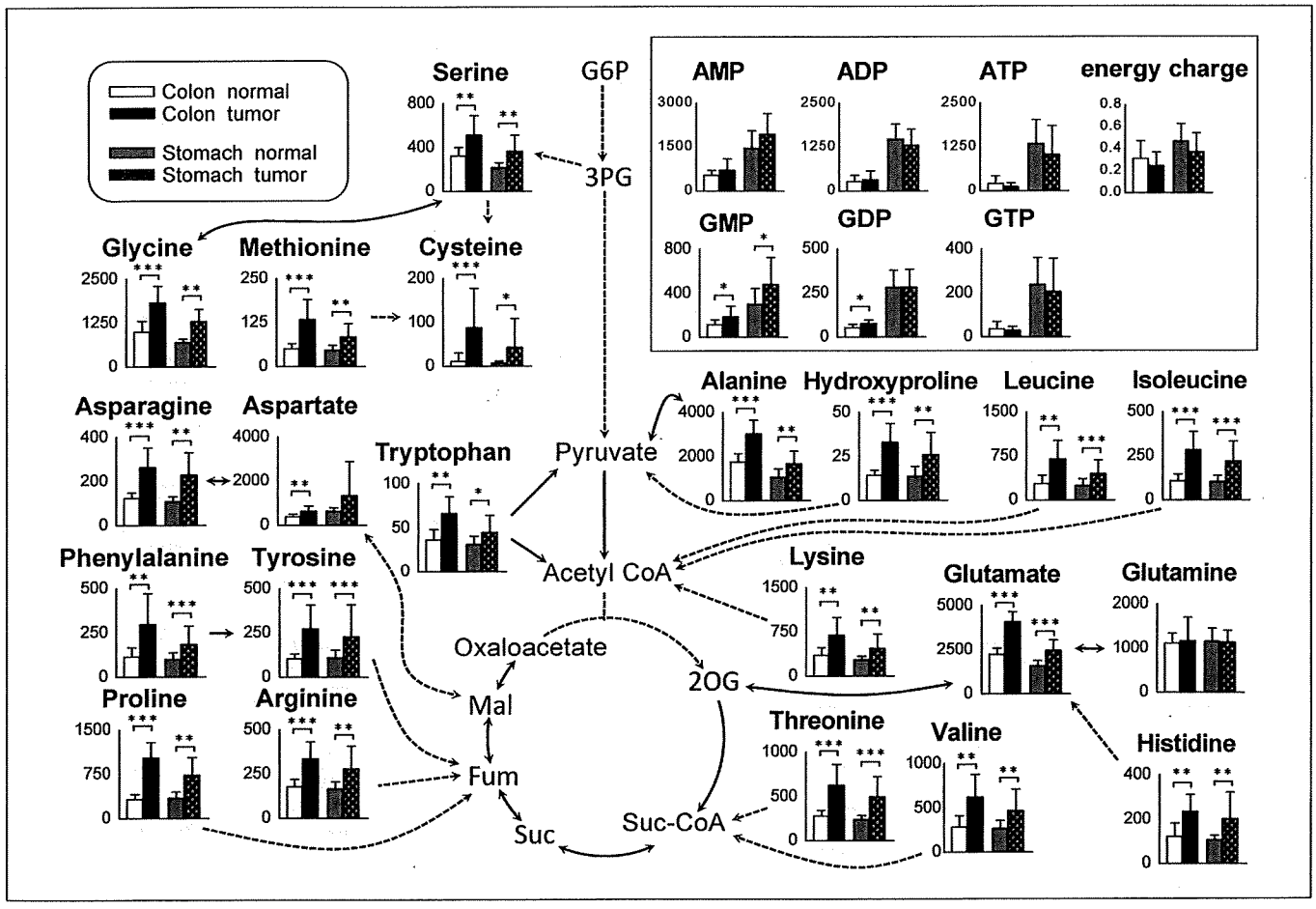

Figure 4. Metabolome data map of metabolites including amino acids, hydroxyproline, and nucleotides (shown in the box) in normal and tumor tissues obtained from colon and stomach cancer patients. *Columns,* average concentration (nmol/g tissue) of normal and tumor tissues; *bars,* SD. *N.D.,* the metabolite concentration was below the detection limit of the analysis. All the P values were evaluated by the Wilcoxon matched pair test. *, $P < 0.05$; **, $P < 0.01$; ***, $P < 0.001$.

metabolisms such as anaerobic glycolysis, glutaminolysis, autophagic production of amino acids, and possibly fumarate respiration, to maintain comparable levels of principal molecules in spite of limited resources and support continuous proliferation.

Intrasample variability and analytic limitations. Biochemical analysis of tissue samples is relatively difficult due to their high heterogeneity compared with cultured cells or body fluids. To examine the intrasample variability, we extracted metabolites from five different parts of a piece of colon or stomach tumor tissue and measured the metabolite levels by CE-TOFMS (Supplementary Table S2). The relative SDs of most metabolite levels were in the range of 6.7% to 40%. Given that the analytic variability of CE-MS is <5% (16), this relatively high intrasample variability may be attributed to a significantly high intratumor heterogeneity. Therefore, to minimize intrasample variability and thus maximize sensitivity for detecting tumor-specific or even tumor-stage specific metabolic differences, the use of laser capture microdissection for concentrating only the target cells before sample homogenization may be promising.

CE-MS is able to simultaneously quantify charged, low–molecular weight compounds and, thus, is suitable for the analysis of primary energy metabolism; however, it is not very effective for the separation of neutral compounds and macromolecules such as sugars, fats, cholesterols, steroid hormones, and long-chain peptides. Concomitant analysis of the same samples by LC-MS, GC-MS, and NMR approaches has the potential to greatly expand the coverage of target compounds and thereby increase the chance of finding molecular fingerprints of tumors and key markers of the tumorigenic process.

In the present study, we analyzed the metabolic state of tumor tissues in comparison with their normal counterparts and found that the nutritional conditions in the tumor microenvironment were far from ideal from the standpoint of energy metabolism. In particular, tumor glucose concentration was significantly lower than previously indicated (44). The results also indicate that tumors develop tumor-specific metabolism that endows them with more predominant proliferation, independent of tissue types, while retaining some metabolic traits of the tissues from which they originated. In other words, cancer cells are evolved through metabolic adaptation that involves primarily hyperactivation of glucose consumption and accumulation of amino acids, while retaining tissue-specific dependency of aerobic respiration represented by TCA intermediate and nucleotide levels. In conclusion, we analyzed the metabolome-wide tumor microenvironment and revealed cancer- and organ-specific characteristic energy metabolism by CE-TOFMS, which will be a vital technology for the future discovery of tissue-specific cancer biomarkers and for the awaited development of novel cancer therapeutic agents that target cancer-specific metabolic traits.

Disclosure of Potential Conflicts of Interest

No potential conflicts of interest were disclosed.

Acknowledgments

Received 12/17/08; revised 3/9/09; accepted 3/20/09; published OnlineFirst 5/19/09.

Grant support: Third Term Comprehensive 10-year Strategy for Cancer Control from the Ministry of Health, Labour and Welfare and a grant from the Global COE Program entitled, "Human Metabolomic Systems Biology." This work was also supported by KAKENHI (Grant-in-Aid for Scientific Research) on Priority Areas "Systems Genomes" and on "Lifesurveyor" from the Ministry of Education, Culture, Sports, Science and Technology of Japan as well as research funds from the Yamagata prefectural government and the City of Tsuruoka.

The costs of publication of this article were defrayed in part by the payment of page charges. This article must therefore be hereby marked *advertisement* in accordance with 18 U.S.C. Section 1734 solely to indicate this fact.

References

1. Vaupel P, Thews O, Kelleher DK, Konerding MA. O2 extraction is a key parameter determining the oxygenation status of malignant tumors and normal tissues. Int J Oncol 2003;22:795–8.
2. Warburg O. On the Origin of Cancer Cells. Science 1956;123:309–14.
3. Chen Z, Lu W, Garcia-Prieto C, Huang P. The Warburg effect and its cancer therapeutic implications. J Bioenerg Biomembr 2007;39:267–74.
4. Kondoh H. Cellular life span and the Warburg effect. Exp Cell Res 2008;314:1923–8.
5. Schauer N, Semel Y, Roessner U, et al. Comprehensive metabolic profiling and phenotyping of interspecific introgression lines for tomato improvement. Nat Biotechnol 2006;24:447–54.
6. Plumb R, Granger J, Stumpf C, Wilson ID, Evans JA, Lenz EM. Metabonomic analysis of mouse urine by liquid-chromatography-time of flight mass spectrometry (LC-TOFMS): detection of strain, diurnal and gender differences. Analyst 2003;128:819–23.
7. Opstad KS, Bell BA, Griffiths JR, Howe FA. An assessment of the effects of sample ischaemia and spinning time on the metabolic profile of brain tumour biopsy specimens as determined by high-resolution magic angle spinning 1H NMR. NMR Biomed 2008;21:1138–47.
8. Yang C, Richardson AD, Smith JW, Osterman A. Comparative metabolomics of breast cancer. Pac Symp Biocomput 2007:181–92.
9. Chan EC, Koh PK, Mal M, et al. Metabolic profiling of human colorectal cancer using high-resolution magic angle spinning nuclear magnetic resonance (HR-MAS NMR) spectroscopy and gas chromatography mass spectrometry (GC/MS). J Proteome Res 2009;8:352–61.
10. Denkert C, Budczies J, Kind T, et al. Mass spectrometry-based metabolic profiling reveals different metabolite patterns in invasive ovarian carcinomas and ovarian borderline tumors. Cancer Res 2006;66:10795–804.
11. Denkert C, Budczies J, Weichert W, et al. Metabolite profiling of human colon carcinoma-deregulation of TCA cycle and amino acid turnover. Mol Cancer 2008;7:72.
12. Soga T, Ohashi Y, Ueno Y, Naraoka H, Tomita M, Nishioka T. Quantitative metabolome analysis using capillary electrophoresis mass spectrometry. J Proteome Res 2003;2:488–94.
13. Soga T, Ueno Y, Naraoka H, Ohashi Y, Tomita M, Nishioka T. Simultaneous determination of anionic intermediates for Bacillus subtilis metabolic pathways by capillary electrophoresis electrospray ionization mass spectrometry. Anal Chem 2002;74:2233–9.
14. Sato S, Soga T, Nishioka T, Tomita M. Simultaneous determination of the main metabolites in rice leaves using capillary electrophoresis mass spectrometry and capillary electrophoresis diode array detection. Plant J 2004;40:151–63.
15. Soga T, Baran R, Suematsu M, et al. Differential metabolomics reveals ophthalmic acid as an oxidative stress biomarker indicating hepatic glutathione consumption. J Biol Chem 2006;281:16768–76.
16. Soga T, Heiger DN. Amino acid analysis by capillary electrophoresis electrospray ionization mass spectrometry. Anal Chem 2000;72:1236–41.
17. Soga T, Ishikawa T, Igarashi S, Sugawara K, Kakazu Y, Tomita M. Analysis of nucleotides by pressure-assisted capillary electrophoresis-mass spectrometry using silanol mask technique. J Chromatogr A 2007;1159:125–33.
18. Smith CA, Want EJ, O'Maille G, Abagyan R, Siuzdak G. XCMS: processing mass spectrometry data for metabolite profiling using nonlinear peak alignment, matching, and identification. Anal Chem 2006;78:779–87.
19. Baran R, Kochi H, Saito N, et al. MathDAMP: a package for differential analysis of metabolite profiles. BMC Bioinformatics 2006;7:530.
20. Saeed AI, Sharov V, White J, et al. TM4: a free, open-source system for microarray data management and analysis. Biotechniques 2003;34:374–8.
21. Koukourakis MI, Pitiakoudis M, Giatromanolaki A, et al. Oxygen and glucose consumption in gastrointestinal adenocarcinomas: correlation with markers of hypoxia, acidity and anaerobic glycolysis. Cancer Sci 2006;97:1056–60.
22. Pedersen PL, Mathupala S, Rempel A, Geschwind JF, Ko YH. Mitochondrial bound type II hexokinase: a key player in the growth and survival of many cancers and an ideal prospect for therapeutic intervention. Biochim Biophys Acta 2002;1555:14–20.
23. Shakoori A, Ougolkov A, Yu ZW, et al. Deregulated GSK3b activity in colorectal cancer: its association with tumor cell survival and proliferation. Biochem Biophys Res Commun 2005;334:1365–73.
24. Koukourakis MI, Giatromanolaki A, Polychronidis A, et al. Endogenous markers of hypoxia/anaerobic metabolism and anemia in primary colorectal cancer. Cancer Sci 2006;97:582–8.
25. Mazzanti R, Solazzo M, Fantappie O, et al. Differential expression proteomics of human colon cancer. Am J Physiol Gastrointest Liver Physiol 2006;290:G1329–38.

26. Argilés JM, Azcón-Bieto J. The metabolic environment of cancer. Mol Cell Biochem 1988;81:3–17.
27. Pan JG, Mak TW. Metabolic targeting as an anticancer strategy: dawn of a new era? Sci STKE 2007;381:pe14.
28. Brahimi-Horn MC, Chiche J, Pouysségur J. Hypoxia signalling controls metabolic demand. Curr Opin Cell Biol 2007;19:223–9.
29. Lu J, Kunimoto S, Yamazaki Y, Kaminishi M, Esumi H. Kigamicin D, a novel anticancer agent based on a new anti-austerity strategy targeting cancer cells' tolerance to nutrient starvation. Cancer Sci 2004;95:547–52.
30. Wiesner RJ, Kreutzer U, Rosen P, Grieshaber MK. Subcellular distribution of malate-aspartate cycle intermediates during normoxia and anoxia in the heart. Biochim Biophys Acta 1988;936:114–23.
31. Kita K, Hirawake H, Miyadera H, Amino H, Takeo S. Role of complex II in anaerobic respiration of the parasite mitochondria from Ascaris suum and Plasmodium falciparum. Biochim Biophys Acta 2002;1553: 123–39.
32. Ullmann R, Gross R, Simon J, Unden G, Kroger A. Transport of C4-dicarboxylates in Wolinella succinogenes. J Bacteriol 2000;182:5757–64.
33. Medina MA, Sánchez-Jiménez F, Márquez J, Rodríguez Quesada A, Núñez de Castro I. Relevance of glutamine metabolism to tumor cell growth. Mol Cell Biochem 1992; 113:1–15.
34. Moreadith RW, Lehninger AL. The pathways of glutamate and glutamine oxidation by tumor cell mitochondria. Role of mitochondrial NAD(P)+-dependent malic enzyme. J Biol Chem 1984;259:6215–21.
35. Phang JM, Donald SP, Pandhare J, Liu Y. The metabolism of proline, a stress substrate, modulates carcinogenic pathways. Amino Acids 2008;35:681–90.
36. Droge W. Autophagy and aging-importance of amino acid levels. Mech Ageing Dev 2004;125:161–8.
37. Mizushima N, Klionsky DJ. Protein turnover via autophagy: implications for metabolism. Annu Rev Nutr 2007;27:19–40.
38. Sato K, Tsuchihara K, Fujii S, et al. Autophagy is activated in colorectal cancer cells and contributes to the tolerance to nutrient deprivation. Cancer Res 2007; 67:9677–84.
39. Fujii S, Mitsunaga S, Yamazaki M, et al. Autophagy is activated in pancreatic cancer cells and correlates with poor patient outcome. Cancer Sci 2008;99:1813–9.
40. Chapman AG, Fall L, Atkinson DE. Adenylate energy charge in Escherichia coli during growth and starvation. J Bacteriol 1971;108:1072–86.
41. Buckstein MH, He J, Rubin H. Characterization of nucleotide pools as a function of physiological state in *Escherichia coli*. J Bacteriol 2008;190:718–26.
42. Hisanaga K, Onodera H, Kogure K. Changes in levels of purine and pyrimidine nucleotides during acute hypoxia and recovery in neonatal rat brain. J Neurochem 1986;47:1344–50.
43. Chapman AG, Atkinson DE. Stabilization of adenylate energy charge by the adenylate deaminase reaction. J Biol Chem 1973;248:8309–12.
44. Gatenby RA, Smallbone K, Maini PK, et al. Cellular adaptations to hypoxia and acidosis during somatic evolution of breast cancer. Br J Cancer 2007;97:646–53.

Anal. Chem. **2009**, *81*, 6165–6174

Metabolomic Profiling of Anionic Metabolites by Capillary Electrophoresis Mass Spectrometry

Tomoyoshi Soga,*,† Kaori Igarashi,† Chiharu Ito,† Katsuo Mizobuchi,‡ Hans-Peter Zimmermann,§ and Masaru Tomita†

Institute for Advanced Biosciences, Keio University, Tsuruoka, Yamagata 997-0052, Japan, Agilent Technologies, 9-1 Takakura-cho, Hachioji, Tokyo 192-8510, Japan, and Agilent Technologies, Hewlett-Packard-Strasse 8, 76337 Waldbronn, Germany

We describe a sheath flow capillary electrophoresis time-of-flight mass spectrometry (CE-TOFMS) method in the negative mode using a platinum electrospray ionization (ESI) spray needle, which allows the comprehensive analysis of anionic metabolites. The material of the spray needle had significant effect on the measurement of anions. A stainless steel spray needle was oxidized and corroded at the anodic electrode due to electrolysis. The precipitation of iron oxides (rust) plugged the capillary outlet, resulting in shortened capillary lifetime. Many anionic metabolites also formed complexes with the iron oxides or migrating nickel ion, which was also generated by electrolysis and moved toward the cathode (the capillary inlet). The metal−anion complex formation significantly reduced detection sensitivity of the anionic compounds. The use of a platinum ESI needle prevented both oxidation of the metals and needle corrosion. Sensitivity using the platinum needle increased from several- to 63-fold, with the largest improvements for anions exhibiting high metal chelating properties such as carboxylic acids, nucleotides, and coenzyme A compounds. The detection limits for most anions were between 0.03 and 0.87 μmol/L (0.8 and 24 fmol) at a signal-to-noise ratio of 3. This method is quantitative, sensitive, and robust, and its utility was demonstrated by the analysis of the metabolites in the central metabolic pathways extracted from mouse liver.

Metabolism is the entire network of chemical reactions that occur in a cell in order to maintain life, in which one metabolite is transformed into another by a sequence of enzymes. Among the whole cellular metabolic network, central carbon metabolism, composed of glycolysis, the pentose phosphate pathway, and the tricarboxylic acid (TCA) cycle, plays key functions in substrate degradation, energy and cofactor regeneration, and biosynthetical precursor supply (DNA, RNA, proteins, peptideglycan, and lipid bilayers).[1,2] Interestingly, all the components involved in the central carbon and energy metabolism are negatively charged: phosphorylated saccharides, phosphorylated carboxylic acids, carboxylic acids, coenzyme A (CoA) compounds, nucleotides, and nicotinamide adenine dinucleotides.

As the importance of metabolomics is recognized, several large-scale metabolite analysis methods using GC/MS,[3] LC/MS,[2,4,5] NMR[6−8] or Fourier transform ion cyclotron resonance mass spectrometry (FTICR-MS)[9,10] have been developed. However, only a limited number of methodologies enable the simultaneous analysis of the anionic metabolites due to their extremely large physicochemical diversity.

Recently, approaches based on capillary electrophoresis mass spectrometry (CE-MS)[11,12] and CE time-of-flight mass spectrometry (CE-TOFMS)[13] have emerged as powerful tools for the comprehensive analysis of charged metabolites and have played a critical role in understanding intricate biochemical and biological systems.[13−19]

* To whom correspondence should be addressed. Phone: (+81) 235 29 0528. Fax: (+81) 235 29 0574. E-mail: soga@sfc.keio.ac.jp.

† Keio University.

‡ Agilent Technologies, Japan.

§ Agilent Technologies, Germany.

10.1021/ac900675k CCC: $40.75
Published on Web 06/12/2009

(1) Sonenshein, A. L. *Nat. Rev. Microbiol.* **2007**, *5*, 917–927.
(2) Yang, W. C.; Sedlak, M.; Regnier, F. E.; Mosier, N.; Ho, N.; Adamec, *J. Anal. Chem.* **2008**, *80*, 9508–9516.
(3) Fiehn, O.; Kopka, J.; Dormann, P.; Altmann, T.; Trethewey, R. N.; Willmitzer, L. *Nat. Biotechnol.* **2000**, *18*, 1157–1161.
(4) Plumb, R.; Granger, J.; Stumpf, C.; Wilson, I. D.; Evans, J. A.; Lenz, E. M. *Analyst* **2003**, *128*, 819–823.
(5) Yoshida, H.; Mizukoshi, T.; Hirayama, K.; Miyano, H. *J. Agric. Food Chem.* **2007**, *55*, 551–560.
(6) Reo, N. V. *Drug Chem. Toxicol.* **2002**, *25*, 375–382.
(7) Coën, M.; Lenz, E. M.; Nicholson, J. K.; Wilson, I. D.; Pognan, F.; Lindon, J. C. *Chem. Res. Toxicol.* **2003**, *16*, 295–303.
(8) Coen, M.; Ruepp, S. U.; Lindon, J. C.; Nicholson, J. K.; Pognan, F.; Lenz, E. M.; Wilson, I. D. *J. Pharm. Biomed. Anal.* **2004**, *35*, 93–105.
(9) Aharoni, A.; Ric de Vos, C. H.; Verhoeven, H. A.; Maliepaard, C. A.; Kruppa, G.; Bino, R.; Goodenowe, D. B. *Omics* **2002**, *6*, 217–234.
(10) Hirai, M. Y.; Yano, M.; Goodenowe, D. B.; Kanaya, S.; Kimura, T.; Awazuhara, M.; Arita, M.; Fujiwara, T.; Saito, K. *Proc. Natl. Acad. Sci. U.S.A.* **2004**, *101*, 10205–10210.
(11) Soga, T.; Ohashi, Y.; Ueno, Y.; Naraoka, H.; Tomita, M.; Nishioka, T. *J. Proteome Res.* **2003**, *2*, 488–494.
(12) Edwards, J. L.; Chisolm, C. N.; Shackman, J. G.; Kennedy, R. T. *J. Chromatogr., A* **2006**, *1106*, 80–88.
(13) Soga, T.; Baran, R.; Suematsu, M.; Ueno, Y.; Ikeda, S.; Sakurakawa, T.; Kakazu, Y.; Ishikawa, T.; Robert, M.; Nishioka, T.; Tomita, M. *J. Biol. Chem.* **2006**, *281*, 16768–16776.
(14) Ishii, N.; Nakahigashi, K.; Baba, T.; Robert, M.; Soga, T.; Kanai, A.; Hirasawa, T.; Naba, M.; Hirai, K.; Hoque, A.; Ho, P. Y.; Kakazu, Y.; Sugawara, K.; Igarashi, S.; Harada, S.; Masuda, T.; Sugiyama, N.; Togashi, T.; Hasegawa, M.; Takai, Y.; Yugi, K.; Arakawa, K.; Iwata, N.; Toya, Y.; Nakayama, Y.; Nishioka, T.; Shimizu, K.; Mori, H.; Tomita, M. *Science* **2007**, *316*, 593–597.
(15) Ohashi, Y.; Hirayama, A.; Ishikawa, T.; Nakamura, S.; Shimizu, K.; Ueno, Y.; Tomita, M.; Soga, T. *Mol. Biosyst.* **2008**, *4*, 135–147.
(16) Yoshida, S.; Imoto, J.; Minato, T.; Oouchi, R.; Sugihara, M.; Imai, T.; Ishiguro, T.; Mizutani, S.; Tomita, M.; Soga, T.; Yoshimoto, H. *Appl. Environ. Microbiol.* **2008**, *74*, 2787–2796.

Application of the sheath flow CE-MS to the analysis of anionic metabolites has been successfully performed using the "negative mode" and a cationic polymer coated capillary.[20] This methodology reverses electroosmotic flow (EOF)[21] toward the anode (the MS direction) to prevent a deleterious current drop. The method enabled the large-scale determination of anionic metabolites, however, with limitations. Several anionic metabolites such as citrate, nucleotides, and CoA compounds were not detected or were detected as poorly shaped peaks.[20,22,23] To overcome the problem, a pressure-assisted CE-MS method[24] was used for these analytes.[22,23] While successful, two separate CE-MS methods for anions were necessary,[11] and moreover, these approaches were not ideal. Additionally, the capillaries frequently clogged.

Recently, it was found that these problems were caused by metal ions generated from the stainless steel needle of the electrospray ionization (ESI) sprayer. Iron oxides formed at the capillary outlet, while nickel ions migrated into the separation capillary and formed complexes with many anions. Here, we propose an improved sheath flow CE-MS method for the analysis of anionic metabolites using a platinum ESI spray needle. The platinum material has a low ionization tendency and does not generate metal ions through electrolysis. This approach overcame the problems and provided robust and sensitive analysis of most of the anionic metabolites and was successfully applied to the quantitative analysis of mouse hepatic metabolites in the central carbon and energy metabolic pathways.

EXPERIMENTAL SECTION

Chemicals. Glycerophosphate was purchased from Nacalai Tesque (Kyoto, Japan), 2-morpholinoethanesulfonate (MES, internal standard) from Dojindo (Kumamoto, Japan), and hexakis-(2,2-difluorothoxy)-phosphazene (Hexakis) from SynQuest Laboratories (Alachua, FL). All other reagents were obtained from Sigma-Aldrich (St. Louis, MO) or Wako (Osaka, Japan). Individual stock solutions of carboxylic acids, phosphorylated saccharides, and phosphorylated carboxylic acids were prepared at a concentration of 100 mM, and stock solutions for other compounds of 10 mM were prepared in Milli-Q water, except for fumarate and trimesate (reference peak) which were prepared in 0.1 M NaOH and succinyl CoA which was prepared in 0.1 M HCl. The working mixture standard was prepared by diluting these stock solutions with Milli-Q water just before injection. All chemicals were of analytical or reagent grade. Water was purified with a Milli-Q purification system (Millipore, Bedford, MA).

Metabolite Extraction. Liver tissue (approximately 300 mg) was immediately plunged into methanol (1 mL) containing 300 μM each of L-methionine sulfone and 2-morpholinoethanesulfonate (MES) (internal standards) and homogenized for 2 min to inactivate enzymes. Then Milli-Q water (500 μL) was added, 300 μL of the solution was transferred, and 200 μL of chloroform was added and mixed well. The solution was centrifuged at 15 000 rpm for 15 min at 4 °C, and the separated 200 μL aqueous layer was centrifugally filtered through a Millipore 5 kDa cutoff filter to remove proteins. The filtrate (100 μL) was lyophilized and dissolved in 50 μL of Milli-Q water containing reference compounds (200 μM each of trimesate and 3-aminopyrrolidine). The solution (2 μM) was diluted with 18 μL of Milli-Q water and then injected into the CE-TOFMS system.[13]

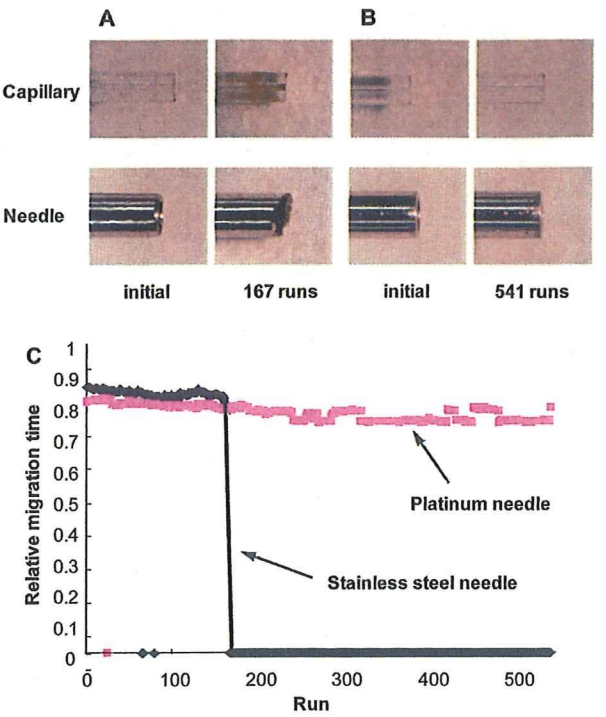

Figure 1. Robustness of the CE-TOFMS system in the anion standard analysis. Photograph of the capillary outlet and the tip of the needle of the COSMO(+) capillary obtained by the CE-ESI-MS sprayer with (A) the SST316Ti stainless steel needle and (B) the platinum needle. (C) Endurance of the system between the SST316Ti stainless steel needle (black) and platinum needle (magenta). The endurance was expressed using the relative migration time of lactate, which was calculated by normalization with the migration time of MES (internal standard). Experimental conditions are described in the Experimental Section.

Instrumentation. All CE-ESI-MS experiments were performed using an Agilent CE capillary electrophoresis system, an Agilent G3250AA LC/MSD TOF system, an Agilent1100 series isocratic HPLC pump, a G1603A Agilent CE-MS adapter kit, and a G1607A Agilent CE-ESI-MS sprayer kit (Agilent Technologies, Waldbronn, Germany). The CE-MS adapter kit includes a capillary cassette which facilitates thermostating of the capillary, and the CE-ESI-MS sprayer kit which simplifies coupling the CE system with MS systems was equipped with an electrospray source. For system control and data acquisition, we used G2201AA Agilent ChemStation software for CE and Agilent TOF (Analyst QS) software for TOFMS.

In addition, the original Agilent SST316Ti stainless steel (Fe/Cr/Ni/Mo/Ti; 68:18:11:2:1) ESI needle was replaced with passivated SST316Ti stainless steel (with 1% formic acid and 20%

(17) Sato, S.; Soga, T.; Nishioka, T.; Tomita, M. *Plant J.* **2004**, *40*, 151–163.
(18) Kinoshita, A.; Tsukada, K.; Soga, T.; Hishiki, T.; Ueno, Y.; Nakayama, Y.; Tomita, M.; Suematsu, M. *J. Biol. Chem.* **2007**, *282*, 10731–10741.
(19) Williams, B. J.; Cameron, C. J.; Workman, R.; Broeckling, C. D.; Sumner, L. W.; Smith, J. T. *Electrophoresis* **2007**, *28*, 1371–1379.
(20) Soga, T.; Ueno, Y.; Naraoka, H.; Ohashi, Y.; Tomita, M.; Nishioka, T. *Anal. Chem.* **2002**, *74*, 2233–2239.
(21) Lukacs, K. D.; Jorgenson, J. W. *J. High Resolut. Chromatogr. Chromatogr. Commun.* **1985**, *8*, 407–411.
(22) Soga, T.; Ueno, Y.; Naraoka, H.; Matsuda, K.; Tomita, M.; Nishioka, T. *Anal. Chem.* **2002**, *74*, 6224–6229.
(23) Soga, T.; Ishikawa, T.; Igarashi, S.; Sugawara, K.; Kakazu, Y.; Tomita, M. *J. Chromatogr., A* **2007**, *1159*, 125–133.
(24) Cao, P.; Moini, M. *Electrophoresis* **1998**, *19*, 2200–2206.

Table 1. Reproducibility, Linearity, and Sensitivity

compound	RSD (n = 8) (%) migration time	RSD (n = 8) (%) peak area	linearity correlation	detection limit (μmol/L)	improved sensitivity ratio[a]
glyoxylate	0.6	11.1	0.997	8.0	0.9
glycolate	0.6	12.4	0.997	5.2	1.7
pyruvate	0.5	8.8	0.999	9.5	0.8
lactate	0.6	5.7	0.985	2.9	1.1
fumarate	0.5	9.4	0.989	0.32	1.4
succinate	0.5	6.3	0.999	0.23	1.6
malate	0.5	4.5	0.994	0.14	4.5
2-oxoglutarate	0.5	5.3	0.985	0.73	4.9
cysteine sulfinate	0.6	6.5	0.998	0.36	4.0
PEP	0.5	5.2	0.995	0.12	3.0
DHAP	0.6	7.8	0.998	0.40	2.2
glycerophosphate	0.6	8.9	0.999	0.46	1.2
cis-aconitate	0.5	7.2	0.997	0.12	4.4
3-phosphoglycerate	0.5	4.9	0.995	0.19	2.8
isocitrate	0.5	3.6	0.996	0.19	6.0
citrate	0.5	7.3	0.988	0.09	63
gluconate	0.7	5.1	0.999	1.1	0.8
E4P	0.6	6.0	0.999	0.81	2.1
Ru5P	0.6	2.7	0.999	0.21	2.4
R5P	0.6	5.1	0.999	0.26	1.9
G1P	0.6	2.1	0.983	0.15	1.9
F6P	0.6	3.5	0.980	0.19	3.4
G6P	0.6	2.4	0.992	0.16	1.6
2,3DPG	0.5	5.8	0.997	0.13	35
6-phosphogluconate	0.5	5.4	0.999	0.18	2.9
F1,6P	0.5	5.4	0.999	0.17	3.1
AMP	0.7	3.5	0.999	0.11	2.1
IMP	0.7	4.8	0.999	0.11	2.9
GMP	0.7	3.6	0.999	0.09	2.0
NADPH[b]	0.6	4.3	0.990	0.45	2.7
CoA[b]	0.6	6.1	0.994	0.03	nc[c]
acetyl CoA[b]	0.6	5.2	0.999	0.04	5.2
malonyl CoA[b]	0.6	6.6	0.995	0.05	7.6
ADP	0.6	3.9	0.995	0.06	5.3
succinyl CoA[b]	0.6	12.1	0.996	0.15	10
GDP	0.6	5.6	0.996	0.11	5.5
UTP	0.6	3.4	0.999	0.10	7.8
ATP	0.6	5.8	0.999	0.22	6.6
GTP	0.6	14.4	0.989	0.10	15
NAD	1.1	4.8	0.999	0.11	1.8
NADH	0.7	3.4	0.999	0.49	11
NADP	0.7	6.1	0.999	0.10	2.4
FAD	0.8	10.5	0.999	0.12	2.8

[a] Improved sensitivity was calculated by dividing the detection limit with the SST316Ti stainless steel by that with the platinum needle. [b] Detected at the divalent $[M - 2H]^{2-}$ ion. [c] nc, not calculated. Improved sensitivity of CoA was not calculated because CoA was not determined by the SST316Ti stainless steel.

isopropanol aqueous solution at 80 °C for 30 min) and platinum. Metal amounts in run buffer solution in the inlet vial and separation capillary were determined using an Agilent 7500 inductivity coupled plasma mass spectrometer (Tokyo, Japan). For the capillary analysis, the polyimide coating was burned with a lighter and removed with methanol, and then the capillary was cut into five pieces (each 20 cm). Each capillary (5.4 mg) was dissolved by ultrasonic treatment in 8 mL of 38% hydrofluoric acid for 80 min, and this solution was used for the inductivity coupled plasma mass spectrometry (ICP-MS) analysis.

CE-TOFMS Conditions for Anionic Metabolite Analysis. A commercially available COSMO(+), chemically coated with a cationic polymer, capillary (50 μm i.d. × 110 cm) (Nacalai Tesque, Kyoto, Japan) was used as the separation capillary. A 50 mM ammonium acetate solution (pH 8.5) was the electrolyte for CE separation. Prior to the first use, a new capillary was flushed successively with the running electrolyte, 50 mM acetic acid (pH 3.4), and then the electrolyte again for 20 min each. Before each injection, the capillary was equilibrated for 2 min by flushing with 50 mM acetic acid (pH 3.4) and then for 5 min by flushing with the running electrolyte.[20]

A sample solution (30 nL) was injected at 50 mbar for 30 s, and −30 kV of voltage was applied. The capillary temperature was thermostated to 20 °C, and the sample tray was cooled to below 5 °C. The Agilent 1100 series pump equipped with a 1:100 splitter was used to deliver 10 μL/min of 5 mM ammonium acetate in 50% (v/v) methanol–water containing 0.1 μM Hexakis to the CE interface where it is used as a sheath liquid around the outside of the CE capillary to provide a stable electrical connection between the tip of the capillary and the grounded electrospray needle.

ESI-TOFMS was conducted in the negative ionization; the capillary voltage was set at 3500 V. For TOFMS, the fragmenter, skimmer, and Oct RFV voltage was set at 100, 50, and 200 V, respectively. A flow rate of drying nitrogen gas (heater temperature, 300 °C) was maintained at 7 L/min. Automatic recalibration

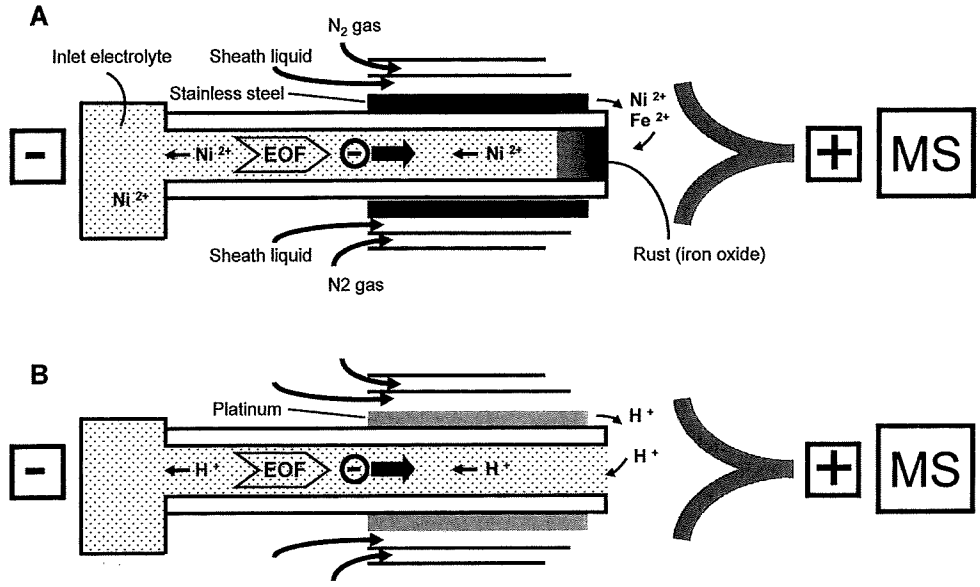

Figure 2. Schematic of anion analysis by the CE-MS in the negative mode using the CE-ESI-MS sprayer with (A) the stainless steel needle and (B) the platinum needle. (A) Metal ions like Fe^{2+} and Ni^{2+} were electrochemically generated from the stainless steel needle at the anode (pH 6.9) and moved into the separation capillary. Fe^{2+} was oxidized (forming rust) and plugged at the capillary outlet due to high electrolyte pH (8.5), while Ni^{2+} migrated toward the capillary inlet (cathode). Anions exhibiting high chelating properties with metal ions formed complexes when encountering Ni^{2+} or iron oxides. (B) In the platinum needle, water oxidation ($2H_2O \rightarrow 4H^+ + O_2\uparrow + 4e^-$) occurred at the anode and, thus, anionic metabolites did not encounter the metal ions.

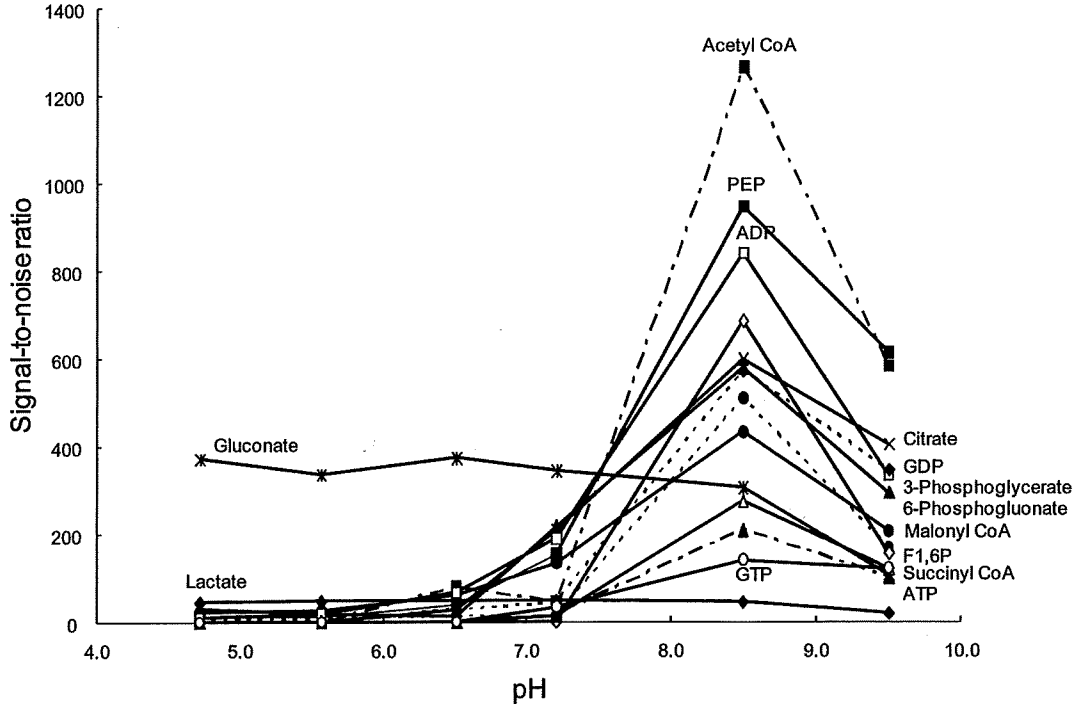

Figure 3. Effect of electrolyte pH on the sensitivity (signal-to-noise ratio) of anions. Experimental conditions: ESI spray needle, platinum; electrolyte, 50 mM ammonium acetate; other experimental conditions as in Figure 1.

of each acquired spectrum was performed using reference masses of reference standards ([^{13}C isotopic ion of deprotonated acetic acid dimer $(2CH_3COOH - H)]^-$, m/z 120.03841), and ([Hexakis + deprotonated acetic acid $(CH_3COOH - H)]^-$, m/z 680.03554). Exact mass data were acquired at a rate of 1.5 spectra/s over a 50–1000 m/z range.

Raw CE-TOFMS data were processed using software developed in-house for the quantification of metabolites.[13,25,26] All target metabolites were identified by matching their m/z values and migration times with those of standard compounds. For overall data analysis, three-dimensional representation of CE-TOFMS data was produced using MZmine2 software[27,28] (http://mzmine.sourceforge.net/).

(25) Baran, R.; Kochi, H.; Saito, N.; Suematsu, M.; Soga, T.; Nishioka, T.; Robert, M.; Tomita, M. *BMC Bioinf.* **2006**, *7*, 530.

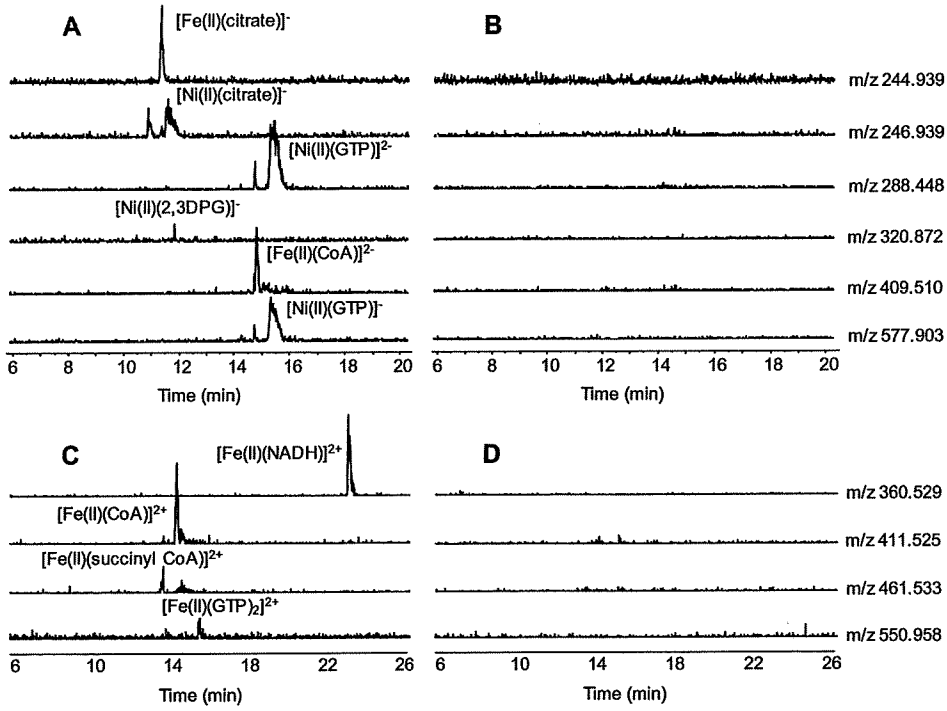

Figure 4. Abundance of metal–anion complexes in the analysis of 43 anionic metabolite standards using CE-TOFMS in the negative mode and negative ionization detection with (A) the stainless steel needle and (B) the platinum needle and positive ionization detection with (C) the stainless steel needle and (D) the platinum needle. Experimental conditions: the names of 43 anionic metabolite standards are listed in Table 1; the standard concentration was 50 μmol/L each; in the positive TOFMS detection, the ion polarity was switched to positive and the capillary voltage was set at 4000 V; other experimental conditions are the same as in Figure 1.

RESULTS AND DISCUSSION

Prevention of Capillary Plugging by Use of a Platinum ESI Needle. The sheath flow CE-MS method with negative mode using a cationic polymer-coated capillary demonstrated impressive performance for anion analysis.[13,20] However, the sensitivities of several anions were considerably poor. Moreover, migration times of every analyte immediately became longer, and the capillary frequently clogged. Removing the polyimide film, we examined a clogged capillary using a microscope and found that the capillary outlet became plugged with a rustlike precipitate. To identify it, we investigated its solubility using several organic solvents and acids including chloroform, isopropanol, acetone, acetonitrile, hydrochloric acid, hydronitric acid, and hydrosulfuric acid. Since it was only soluble in hydrochloric acid, it was identified as a transition metal having a high ionization tendency like iron and nickel.

Although the original Agilent CE-ESI-MS spray needle is made from SST316Ti stainless steel, it exhibited high ionization tendency and, thus, was oxidized to metal ions by electrolysis, resulting in a plug at the capillary outlet. To confirm this, we attached the following three types of spray needles to the Agilent ESI sprayer: normal- and passivated-SST316Ti stainless steel and platinum. Using these spray needles, we performed the CE-MS analyses with the negative mode and checked the capillary outlet with a microscope after 5, 10, and over 40 runs, respectively.

With the two needles made from the stainless steel, both the capillary outlets became plugged with precipitates (rust) after five runs and the rust grew thicker with the number of analysis performed, indicating that electrochemical oxidation of the stainless steel occurred. However, the use of the platinum needle resulted in no plugging for 100 runs. This is consistent with previous reports that platinum wire used as the CE-MS ESI electrode protects against electrode corrosion.[29–32] As Smith and Moini[31] reported, when a stainless steel wire was used as the anode, the oxidation of iron ($Fe \rightarrow Fe^{2+} + 2e^-$) (perhaps Ni, Cr, and Ti) replaced the oxidation of water ($2H_2O \rightarrow 4H^+ + O_2\uparrow + 4e^-$) by electrolysis, resulting in corrosion of the Fe and formation of Fe^{2+}. However, platinum wire only caused electrochemical oxidation of water, and bubble formation occurred at the anodic end.

The robustness of the CE-MS method with the negative mode using the SST316Ti stainless steel needle and platinum needle was further investigated. With the stainless steel needle, both capillary clogging with rust and significant corrosion at the tip of the needle occurred (Figure 1A) and the current fully dropped after 167 runs (Figure 1C). For the platinum needle, although a slight current drop and migration time fluctuation were observed (Figure 1C), it enabled over 545 successive analyses without capillary clogging and corrosion of the needle (Figure 1B). While Smith and Moini used iron wire, instead of platinum wire, as the anode to eliminate gas bubble formation in their sheathless CE-

(26) Hirayama, A.; Kami, K.; Sugimoto, M.; Sugawara, M.; Toki, N.; Onozuka, H.; Kinoshita, T.; Saito, N.; Ochiai, A.; Tomita, M.; Esumi, H.; Soga, T. *Cancer Res.* **2009**, *69*, 4918–4925.
(27) Katajamaa, M.; Oresic, M. *BMC Bioinf.* **2005**, *6*, 179.
(28) Katajamaa, M.; Miettinen, J.; Oresic, M. *Bioinformatics* **2006**, *22* (5), 634–636.
(29) Cao, P.; Moini, M. *J. Am. Soc. Mass Spectrom.* **1997**, *8*, 561–564.
(30) Herring, C. J.; Qin, J. *Rapid Commun. Mass Spectrom.* **1999**, *13*, 1–7.
(31) Smith, A. D.; Moini, M. *Anal. Chem.* **2001**, *73*, 240–246.
(32) Van Berkel, G. J.; Asano, K. G.; Schnier, P. D. *J. Am. Soc. Mass Spectrom.* **2001**, *12*, 853–862.

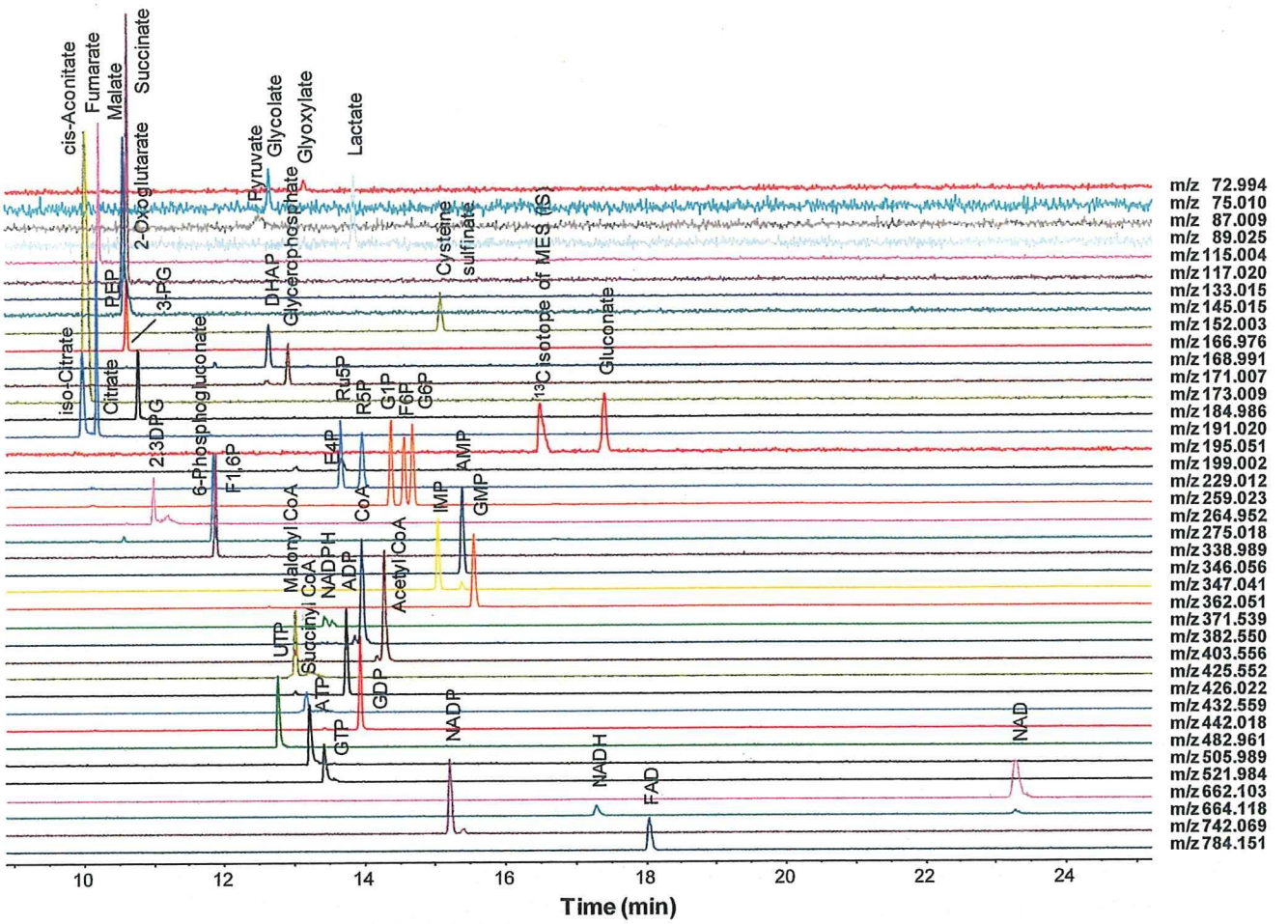

Figure 5. Selected CE-TOFMS ion electropherograms for a standard mixture of anionic metabolites in the components of glycolysis, pentose phosphate, and the TCA pathways obtained by the CE-ESI-MS sprayer attached with a platinum needle. Experimental conditions: standard concentration, 10 μmol/L each; other experimental conditions as in Figure 1. Abbreviations: PEP, phosphoenolpyruvate; DHAP, dihydroxyacetone phosphate; 3PG, 3-phosphoglycerate; E4P, erythrose 4-phosphate; Ru5P, ribulose 5-phosphate; R5P, ribose 5-phosphate; G1P, glucose 1-phosphate; F6P, fructose 6-phosphate; G6P, glucose 6-phosphate; 2,3DPG, 2,3-diphosphoglycerate; F1,6P, fructose 1,6-diphosphate; NADPH, reduced nicotinamide adenine dinucleotide phosphate; NADP, nicotinamide adenine dinucleotide phosphate; FAD, flavin adenine dinucleotide.

MS system,[31] our results indicate that bubble formation generated by the platinum needle had no effect on the analysis in the sheath flow CE-MS system.

Sensitivity Differences between the Stainless Steel Needle and the Platinum Spray Needle in Anion Analysis. There was another difficulty in analyzing anionic metabolites by the CE-MS method with the negative mode using the ESI sprayer equipped with the SST316Ti stainless steel needle. Several carboxylic acids and phosphorylated compounds such as malate, 2-oxoglutarate, 3-phosphoglycerate (3PG), citrate, isocitrate, gluconate, 2,3-diphosphoglycerate (2,3DPG), uridine 5′-triphosphate (UTP), adenosine 5′-triphosphate (ATP), guanosine 5′-triphosphate (GTP), reduced nicotinamide adenine dinucleotide (NADH), coenzyme A (CoA), and acetyl- and malonyl-CoA with a concentration below a few micromolar were not detected. However, all the anions were detected as well-defined peaks with the platinum needle.

Many carboxylic acids and nucleotides such as citrate, malate, ATP, GTP, and NADH are complexing agents,[33−38] which display high stability constants for transition metals. For phosphorylated saccharides and CoAs, stability constants for transition metals have not been frequently reported. However, as metal−phosphate affinity is well-known[33,35,39,40] and these characteristics are frequently utilized in phoshoproteomics studies,[41,42] most phosphorylated compounds will likely interact with transition metals.

Experiments show sensitivity differences between the two needles for metal-chelating carboxylic acids, and phosphorylated anions are observed (Table 1). Conversely, pyruvate, lactate, and fumarate exhibit little or no stability constants for transition metals,[34] and their sensitivities were independent of the needle type. Unlike NADH, nicotinamide adenine dinucleotide (NAD^+)

(33) Toyokuni, S. *Free Radicical Biol. Med.* **1996**, *20*, 553–566.
(34) Soga, T.; Gordon, R. A. *J. Chromatigr., A* **1997**, *767*, 223–230.
(35) Kowaltowski, A. J.; Vercesi, A. E. *Free Radical Biol. Med.* **1999**, *26*, 463–471.
(36) Canaviri, E. C.; Feliz, M. R.; Capparelli, A. L. *Transition Met. Chem.* **1992**, *17*, 446–448.
(37) Champeil, P.; Rigaud, J. L.; Gary-Bobo, C. M. *Proc. Natl. Acad. Sci. U.S.A.* **1980**, *77*, 2405–2409.
(38) Lvovich, V.; Scheeline, A. *Arch. Biochem. Biophys.* **1995**, *320*, 1–13.
(39) Takebayashi, Y.; Mitsuma, R.; Imanari, T. *Anal. Sci.* **1987**, *3*, 569–572.
(40) Ziemniak, S. E.; Jones, M. E.; Combs, K. E. S. *J. Solution Chem.* **1989**, *18*, 1133–1152.
(41) Stensballe, A.; Andersen, S.; Jensen, O. N. *Proteomics* **2001**, *1*, 207–222.
(42) Kokubu, M.; Ishihama, Y.; Sato, T.; Nagasu, T.; Oda, Y. *Anal. Chem.* **2005**, *77*, 5144–5154.

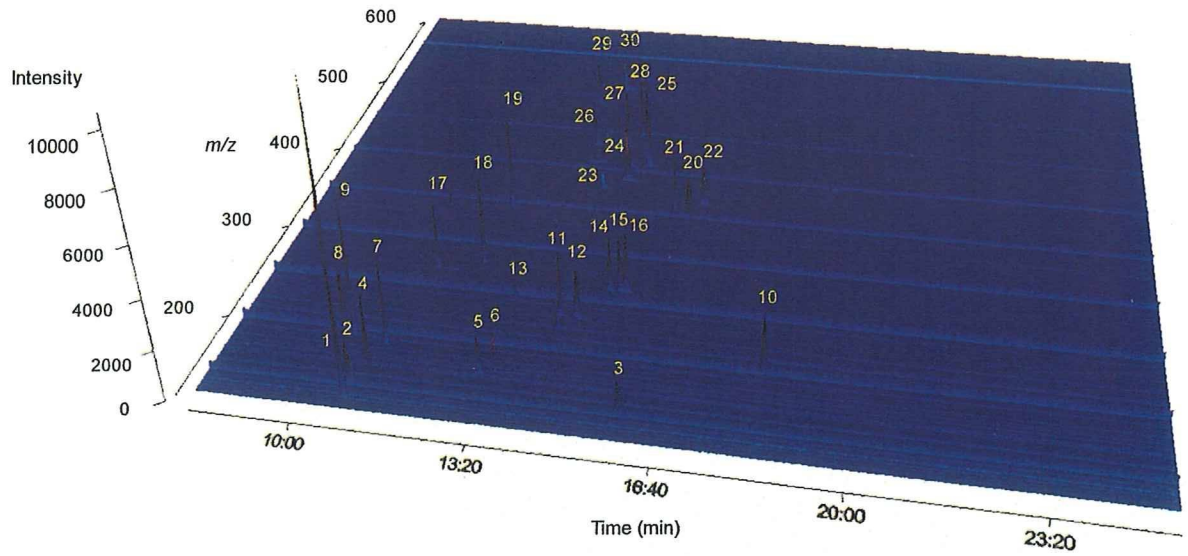

Figure 6. Three-dimensional representation (total ion electropherogram) for the analysis of a standard mixture of anionic metabolites found in glycolysis, pentose phosphate, and the TCA pathways. Results were obtained by the CE-TOFMS in the negative mode using the CE-ESI sprayer with a platinum needle. Experimental conditions: standard concentration, 50 μmol/L each; other experimental conditions are the same as in Figure 1. Peaks: 1, malate; 2, 2-oxoglutarate; 3, cysteine sulfinate; 4, PEP; 5, DHAP; 6, glycerophosphate; 7, 3PG; 8, isocitrate; 9, citrate; 10, gluconate; 11, E4P; 12, Ru5P; 13, R5P; 14, G1P; 15, F6P; 16, G6P; 17, 2,3DPG; 18, 6-phosphogluconate; 19, F1,6P; 20, AMP; 21, IMP; 22, GMP; 23, NADPH; 24, CoA; 25, acetyl CoA; 26, malonyl CoA; 27, ADP; 28, GDP; 29, UTP; 30, ATP.

does not form a complex with the Fe^{2+} ion;[38] thereby, NAD^+'s sensitivity is most similar between the two needles. These facts indicate that the anions' metal-chelating properties likely affect their detection sensitivities.

Effect of Generated Metal Ions on Sensitivity in Measurement of Anionic Metabolites. To investigate the hypothesis that anionic metabolites exhibiting high stability constants for metal ions might form complexes with the iron oxides generated by the stainless steel needle, the separation capillary was cut into five pieces (each 20 cm) and analyzed by ICP-MS. The ICP-MS analysis detected a 10.4 ppb level of Fe in the tip of the capillary outlet (the anode side), which identified the rust as iron oxide, but no metals in other regions of the capillary. Surprisingly, nickel was detected in the capillary inlet electrolyte, and its concentration dramatically increased (0.96 μg/L at 1 h and reached 3.08 μg/L at 2 h) even when no sample was injected. This indicates that nickel ion migrated from the anode to the inlet electrolyte vial. However, no such phenomena were observed when using the platinum needle.

It is, therefore, assumed that, with the stainless steel needle (Figure 2A), iron and nickel ions generated at the anode due to electrolysis moved to the capillary outlet in the sheath liquid (pH 6.9) and iron oxides formed because of the high pH (pH 8.5)[20] (Figure 3). Simultaneously, Ni^{2+} ions migrated toward the cathode without precipitation and then collected in the capillary inlet electrolyte vial. In this manner, injected anionic metabolites encountered Ni^{2+} in the separation capillary or the iron oxides at the capillary end and formed metal–anion complexes (Figure 2A). In the case of the platinum needle, water oxidation ($2H_2O \rightarrow 4H^+ + O_2\uparrow + 4e^-$) occurred at the anode due to its low ionization tendency and anionic metabolites did not encounter the metal ions and were fully detected by the mass spectrometer (Figure 2B).

The formation of metal–anion complexes during the CE-MS analysis was also confirmed. As listed in Table 1, when the stainless steel needle was used, a significant drop in sensitivity was observed for many anions including citrate, 2,3DPG, GTP, CoA, succinyl CoA, and NADH. For these anions, the formation of all nickel(II)– and iron(II)–anion complexes was analyzed by the CE-TOFMS method. In the negative ionization TOFMS method, nickel(II)– and iron(II)–anion complexes such as $[Fe(II)-(citrate)]^-$, $[Ni(II)-(citrate)]^-$, $[Ni(II)-(GTP)]^{2-}$, $[Ni(II)-(2,3DPG)]^-$, $[Fe(II)-(CoA)]^{2-}$, and $[Ni(II)-(GTP)]^-$ were detected with the stainless steel needle (Figure 4A). Moreover, positively charged nickel(II)– and iron(II)–anion complexes such as $[Fe(II)-(NADH)]^{2+}$, $[Fe(II)-(CoA)]^{2+}$, $[Fe(II)-(succinyl\ CoA)]^{2+}$, and $[Fe(II)-(GTP)_2]^{2+}$ were present in the positive ionization TOFMS detection (Figure 4C). These results indicate that all the anions formed complexes with nickel(II) and iron(II) ions with the stainless steel needle. No metal complexes were observed with the platinum needle (Figure 4B,D).

It was found, however, that the sensitivities for pyruvate, lactate, and fumarate were equivalent using either the stainless steel or platinum needle (Table 1). Although a trace of $[Fe(II)-(pyruvate)_3]^-$ was detected with the stainless steel needle, neither these nickel(II)– nor iron(II)–anion complexes were detected with either needle. These results indicate that with the stainless steel needle, anions exhibiting high stability constants with metals formed complexes with nickel and iron ions generated by electrolysis, resulting in a significant decrease in detection sensitivity.

Effect of Electrolyte pH on Rust Formation and Sensitivity in the CE-MS System. Given that iron ions generated from the stainless steel needle precipitated when encountering the alkaline electrolyte (pH 8.5), they are expected to be dissolved under acidic conditions. To confirm this, iron oxide formation was studied over

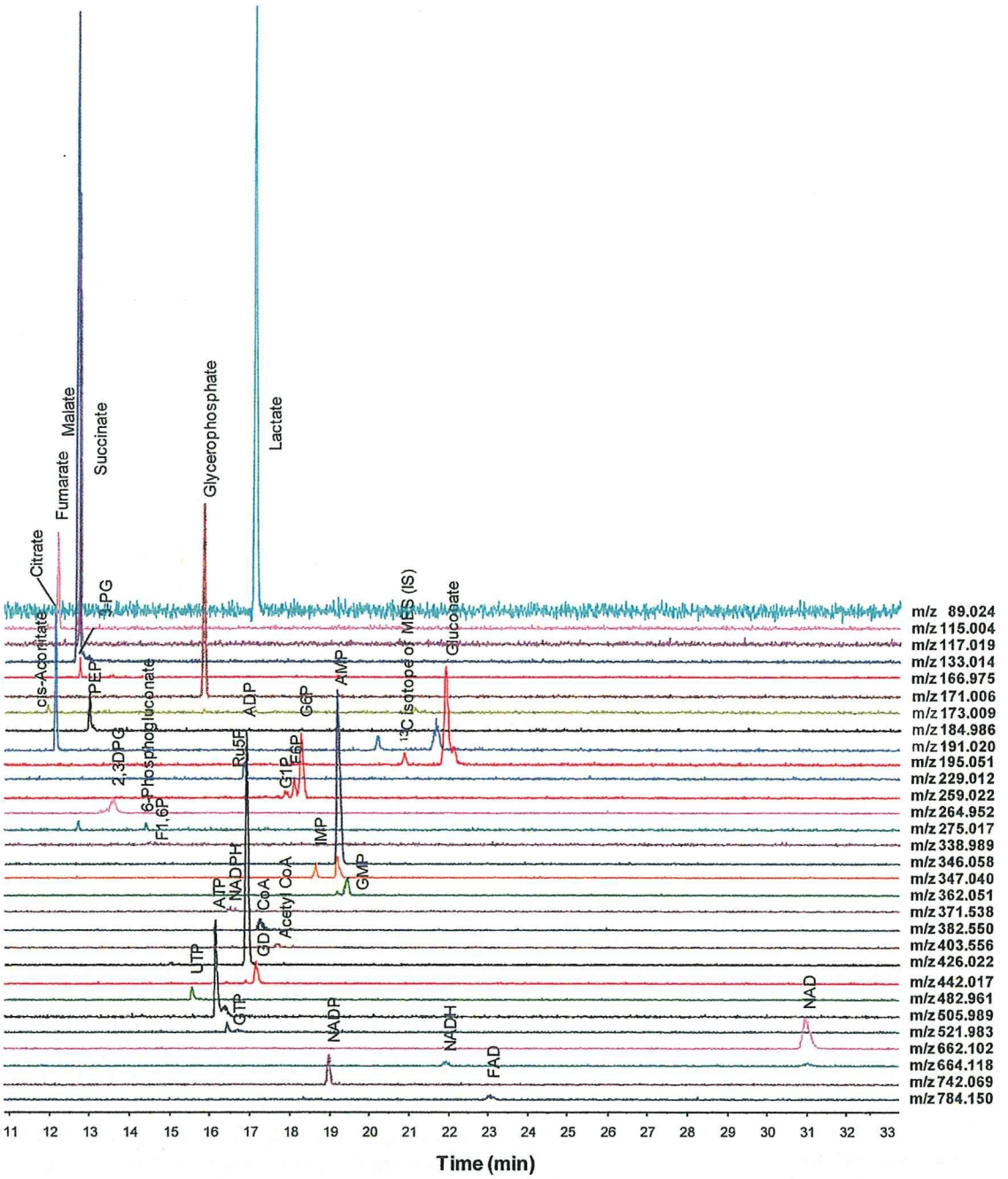

Figure 7. Selected CE-TOFMS ion electropherograms for components of glycolysis, pentose phosphate, and the TCA pathways in mouse liver. Experimental conditions are the same as in Figure 1.

pH range 4.7–9.5 using 50 mM ammonium acetate as the electrolyte and the stainless steel needle. At a pH value of 7.5, both rust development at the capillary end and corrosion of the stainless steel needle were observed. At pH 5.0, although corrosion of the needle was still observed, no iron oxide was formed. After the voltage was applied (no sample injection) for 2 h at the pH 5.0, metals at the capillary inlet electrolyte were analyzed by ICP-MS. Fe, Ni, and Ti, some components of the SST316Ti stainless steel, were detected at amounts of 1.23, 0.88, and 0.24 μg/L, respectively, which strongly implies that these metal ions were generated by electrolysis and migrated toward the cathodes.

Nevertheless, decreasing electrolyte pH had a significant effect on the detection sensitivity of anionic species (Figure 3). Below pH 7.5, although the reason was unclear, a considerable deterioration in the peak shape and extended migration time of many anions including phosphorylated substrates, nucleotide di- and triphosphates, and CoAs were observed, which resulted in substantial reduction in their detection sensitivity. Particularly, neither nucleotide triphosphates nor CoAs were detected below pH 6.5. Sensitivities of anions also decreased when the pH was increased to pH 9.5. Maximal sensitivities for most anions were obtained at pH 8.5 (Figure 3). This result was independent of the ESI needle type used. Reduction of sensitivity depending on the pH may be caused by the interaction between these compounds and the cationic coated polymer on the capillary wall, though further investigation is necessary.

In conclusion, there is no pH that can be used with the stainless steel needle to both prevent iron oxide formation and maintain

Table 2. Metabolite Amount, Reproducibility, and Recovery in Mouse Liver Analysis

compound	amount (nmol/g)	RSD (n = 12) (%)	recovery rate (average, n = 5) (%)
glyoxylate	nd[a]		106
glycolate	nd		117
pyruvate	nd		138
lactate	2440	5.7	67
fumarate	247	8.4	99
succinate	526	4.9	65
malate	1250	2.6	53
2-oxoglutarate	nd		94
cysteine sulfinate	nd		101
PEP	44	7.8	96
DHAP	nd		100
glycerophosphate	1310	3.9	97
cis-aconitate	6.0	15.6	141
3-phosphoglycerate	159	5.0	103
isocitrate	nd		103
citrate	264	6.1	89
gluconate	675	4.5	109
E4P	nd		114
Ru5P	68	11.1	101
R5P	nd		98
G1P	34	12.7	97
F6P	98	7.0	92
G6P	392	4.7	95
2,3DPG	215	5.1	93
6-phosphogluconate	23	21.9	97
F1,6P	22	15.8	92
AMP	1240	2.1	96
IMP	81	7.9	98
GMP	143	4.8	93
NADPH (divalent)	66	16.5	146
CoA (divalent)	68	10.0	132
acetyl CoA (divalent)	14	15.4	96
malonyl CoA (divalent)	nd		110
ADP	1500	4.7	88
succinyl CoA (divalent)	nd[a]		58
GDP	181	3.0	94
UTP	89	15.3	94
ATP	889	3.8	120
GTP	149	6.2	183
NAD	494	3.7	93
NADH	166	7.2	114
NADP	184	4.9	90
FAD	47	7.5	92

[a] nd, not detected.

peak shape for necessary detection sensitivity. For the platinum needle, pH 8.5 was found optimal.

Method Validation. Figure 5 illustrates selected ion electropherograms of the 43 anionic metabolite standards in the components of glycolysis, pentose phosphate, and the tricarboxylic acid (TCA) pathways obtained by the sheath flow CE-TOFMS with the negative mode using the platinum spray needle. A three-dimensional presentation (total ion electropherogram) is shown in Figure 6. This analysis will be particularly important to analyze unknown metabolites. This approach provided much better sensitivity and, thereby, contributed to excellent performance, compared to the previous method. Most of compounds were detected at their monovalent deprotonated molecular $[M - H]^-$ ions, while intensity in the divalent $[M - 2H]^{2-}$ ion of NADPH and CoA compounds was higher than that in monovalent ion.

The reproducibility, linearity, and sensitivity of this method are listed in Table 1. Practical reproducibility was obtained for all anionic species with relative standard deviation (RSD) values (n = 8) for migration times between 0.5 and 1.1% and for peak areas better than 10% except for glyoxylate, glycolate, succinyl CoA, GTP, and FAD, as indicated in the table. The calibration curves for all species were linear at 1, 2, 5, 10, 20, 50, 100, and 200 μmol/L with correlation coefficients between 0.980 and 0.999.

This method significantly improved the sensitivity of many anions. Although the previous method using the stainless steel needle was unable to detect 20 μmol/L of CoA, the use of the platinum needle dramatically improved sensitivity and enabled the detection of 1 μmol/L of CoA. Moreover, the sensitivities for the anions exhibiting high stability constants for metal ions such as citrate, 2,3DPG, GTP, and NADH were 63-, 35-, 15-, and 11-fold superior to those obtained by the stainless steel needle, respectively. Also several-fold better sensitivities for many anions including malate, 2-oxoglutarate, *cis*-aconitate, isocitrate, ADP, ATP, GDP, UTP, and succinyl-, acetyl-, and malonyl CoA were obtained.

Anions exhibiting low stability constants with metals such as pyruvate and lactate showed similar sensitivities between the two needles. Overall, the concentration detection limits for most of the anions, except for glyoxylate, glycolate, pyruvate, and lactate, were between 0.03 and 1.1 μmol/L with a pressure injection of 50 mbar for 30 s (30 nL); i.e., mass detection limits ranged from 0.8 to 33 fmol, at a signal-to-noise ratio of 3.

Analysis of Mouse Liver Metabolites in the Central Carbon and Energy Metabolism. The utility of the CE-TOFMS method was demonstrated by the simultaneous analysis of the central carbon and energy metabolism components extracted from mouse liver. There are more than 40 anionic intermediates that belong to several categories of chemical compounds: phosphorylated saccharides, phosphorylated carboxylic acids, carboxylic acids, nucleotides, and cofactors. Simultaneous, quantitative, and direct analysis of these compounds is a challenging analytical problem. Figure 7 shows the results for the analysis of the central carbon and energy metabolic components extracted from mouse livers obtained by the CE-TOFMS method. The 32 components were identified by comparing their molecular weights and migration times with those of metabolite standards, and their amounts were quantified by their standard calibration curves (Table 1). The relative standard deviations (n = 12) for the amounts of identified compounds in the mouse liver sample were better than 6% except for small compounds. To investigate quantification accuracy and ion suppression effect in this system, we analyzed mouse liver samples spiked with 20 μM of each standard and calculated the recovery (Table 2). Except for a few metabolites, the recovery rates of most metabolites in the CE-TOFMS approach were between 80 and 130%. Although the reason was not clear, the recovery rate of GTP was unusually high (183%). Considering the good reproducibility and recovery rates, the CE-TOFMS method in the negative mode using the platinum spray needle seems to be scarcely affected by the ion suppression effect and it enables sufficient quantitative analysis of most anionic intermediates in the central carbon and energy metabolic pathways extracted from mouse liver samples.

CONCLUSIONS

A negatively charged metabolites profiling approach based on sheath flow CE-TOFMS with a negative mode is described. The material of the ESI spray needle had a significant effect

on the measurement of anions. Due to electrolysis, the stainless steel sprayer needle was easily oxidized and generated metal ions, which caused corrosion of the needle and capillary clogging. Moreover, metal ions formed complexes with many anions, significantly decreasing detection sensitivity. The key to success was using a platinum spray needle, a low ionization tendency metal, which prevented both generation of metal ions and corrosion of the needle caused by electrolysis. Compared with the previously reported techniques, this method has several advantages: (1) it is able to integrate two CE-MS methods into one method, and thereby, all types of anionic components such as phosphorylated saccharides, phosphorylated carboxylic acids, carboxylic acids, CoA compounds, nucleotides, and nicotinamide adenine dinucleotides are simultaneously analyzed; (2) more than several-fold increased sensitivities of anions which exhibit high metal chelating properties are obtained; and (3) the present method provides improved reproducibility, quantification accuracy, and method robustness (i.e., capillary lifetime). Its utility was demonstrated by the simultaneous and quantitative analysis of the central carbon and the energy the metabolic intermediates extracted from mouse livers. These results indicate that the proposed CE-TOFMS method can be useful for the comprehensive analysis of anionic species in a wide range of application areas.

ACKNOWLEDGMENT

We thank Akiyoshi Hirayama and Dr. Masahiro Sugimoto, Institute for Advanced Biosciences, Keio University, and Takamasa Ishikawa, Human Metabolome Technologies Inc., for technical support, and Dr. David N. Heiger, Agilent Technologies, for critical reading of the manuscript. This work was supported in part by grants for the Health and Labour Sciences Research Grants entitled "Research on Risk of Chemical Substances" and "Research on Biological Markers for Drug development", by a Grant-in-Aid for Creative Scientific Research 17GS0419 from the Japan Society for the Promotion of Science, by a grant from the Global COE Program entitled "Human Metabolic System Biology", and by a Grant-in-Aid for Scientific Research on Priority Areas "Life surveyor" and "Systems Genomes" from the Ministry of Education, Culture, Sport, Science, and Technology (MEXT) in Japan as well as by research funds from Yamagata prefectural government and Tsuruoka city.

Received for review March 31, 2009. Accepted May 31, 2009.

AC900675K